Acta Biomaterialia xxx (xxxx) xxx

Contents lists available at ScienceDirect

Acta Biomaterialia

journal homepage: www.elsevier.com/locate/actbio

Full length article

A Gaussian process approach for rapid evaluation of skin tension

Matt Nagle[a,b,*], Hannah Conroy Broderick[b], Christelle Vedel[b,c], Michel Destrade[b,d], Michael Fop[e,1,*], Aisling Ní Annaidh[b,f,1,*]

[a] SFI Centre for Research Training in Foundations of Data Science, University College Dublin, Belfield, Dublin 4, Ireland
[b] School of Mechanical and Materials Engineering, University College Dublin, Belfield, Dublin 4, Ireland
[c] EPF School of Engineering, Av. du Président Wilson, Cachan, France
[d] School of Mathematical and Statistical Sciences, University of Galway, University Rd, Galway, Ireland
[e] School of Mathematics and Statistics, University College Dublin, Belfield, Dublin 4, Ireland
[f] Charles Institute of Dermatology, University College Dublin, Belfield, Dublin 4, Ireland

ARTICLE INFO

Article history:
Received 15 February 2024
Revised 17 April 2024
Accepted 10 May 2024
Available online xxx

Keywords:
Skin tension
Non-invasive
Rayleigh surface wave
Supersonic shear wave
Finite element simulations
Machine learning

ABSTRACT

Skin tension plays a pivotal role in clinical settings, it affects scarring, wound healing and skin necrosis. Despite its importance, there is no widely accepted method for assessing *in vivo* skin tension or its natural pre-stretch. This study aims to utilise modern machine learning (ML) methods to develop a model that uses non-invasive measurements of surface wave speed to predict clinically useful skin properties such as stress and natural pre-stretch. A large dataset consisting of simulated wave propagation experiments was created using a simplified two-dimensional finite element (FE) model. Using this dataset, a sensitivity analysis was performed, highlighting the effect of the material parameters and material model on the Rayleigh and supersonic shear wave speeds. Then, a Gaussian process regression model was trained to solve the ill-posed inverse problem of predicting stress and pre-stretch of skin using measurements of surface wave speed. This model had good predictive performance ($R^2 = 0.9570$) and it was possible to interpolate simplified parametric equations to calculate the stress and pre-stretch. To demonstrate that wave speed measurements could be obtained cheaply and easily, a simple experiment was devised to obtain wave speed measurements from synthetic skin at different values of pre-stretch. These experimental wave speeds agree well with the FE simulations, and a model trained solely on the FE data provided accurate predictions of synthetic skin stiffness. Both the simulated and experimental results provide further evidence that elastic wave measurements coupled with ML models are a viable non-invasive method to determine *in vivo* skin tension.

Statement of significance

To prevent unfavourable patient outcomes from reconstructive surgery, it is necessary to determine relevant subject-specific skin properties. For example, during a skin graft, it is necessary to estimate the pre-stretch of the skin to account for shrinkage upon excision. Existing methods are invasive or rely on the experience of the clinician. Our work aims to present an innovative framework to non-invasively determine *in vivo* material properties using the speed of a surface wave travelling through the skin. Our findings have implications for the planning of surgical procedures and provides further motivation for the use of elastic wave measurements to determine *in vivo* material properties.

1. Introduction

The skin is the largest organ in the body and serves as the interface between the internal physiological environment and the external world. It plays a pivotal role in protection against external threats, including the invasion of pathogens and fending off chem-

* Corresponding authors at: School of Mathematical and Statistical Sciences, UCD, Belfield, Dublin 4, Ireland.
E-mail addresses: matt.nagle@ucdconnect.ie (M. Nagle), michael.fop@ucd.ie (M. Fop), aisling.niannaidh@ucd.ie (A. Ní Annaidh).
[1] These authors contributed equally to this work.

https://doi.org/10.1016/j.actbio.2024.05.025

ical and physical assaults [1]. It is under constant anisotropic tension and must be both pliable and durable for everyday movement.

In the surgical setting, skin tension plays a crucial role in achieving optimal outcomes and fostering effective wound healing processes [2,3]. In many surgical procedures, such as wound closure or breast reconstructions, maintaining appropriate skin tension is paramount. Excessive tension can lead to complications such as compromised aesthetics and scarring [3,4], and further, to significant psychosocial impacts for the patient [5]. It can also lead to dangerous physical complications including wound dehiscence, haematoma and skin necrosis, which can occur at alarmingly high complication rates for patients. For example, recent publications have reported overall complication rates for head and neck tissue expansion of 8.73% [6] and that 8.9% of patients experience skin necrosis from breast tissue expansion following a mastectomy [7].

It is well established that *in vivo* skin tension is aligned along preferred directions known as Langer lines, skin tension lines or relaxed skin tension lines [3,8,9]. Both the magnitude of *in vivo* skin tension and its preferred orientation have been shown to be patient-specific [10,11]. However, despite the important role skin tension plays in surgery, there is no commonly accepted quantitative method to determine its magnitude or direction *in vivo*. Currently, surgeons must rely on generic skin tension maps or an imprecise "pinch test" to identify the orientation of skin tension lines, which requires significant skill and experience to interpret [10,12,13].

Recently, attempts have been made to identify the *direction* of skin tension lines using suction devices [14], extensiometry [15,16] and elastic wave propagation [10,17]. There have also been attempts to quantify the *magnitude* of *in vivo* pre-stretch and skin tension. However, many of the methods are invasive and cumbersome and have not been widely adopted [10,18–20].

Most methods to determine the magnitude of pre-stretch involve a destructive process where the skin is excised, and the shrinkage is quantified [10,18,19]. A notable exception is the method employed by Paul et al. where instead of skin being excised, rods are used to compress or stretch the skin [20]. However, the measurement process is still invasive, as the rods must pierce the skin for a measurement to be taken.

Our own recent publication analysed the direction and relative magnitude of skin tension using a wave propagation device (Reviscometer® Model RVM 600, made by Courage & Khazaka Electronic GmbH) to take *in vivo* measurements of the surface wave speed [11]. Devices such as these can be made easily and cheaply to facilitate measurements of wave speed on the surface of the skin along one axis. They often contain two piezoelectric transducers spaced a known distance apart. One transducer impacts the surface of the material, generating a surface wave, while the other transducer detects the resulting wave and records the time taken for that wave to propagate across the surface of the skin, along one axis. We demonstrated that the direction of highest skin tension and its magnitude is subject specific and is affected by the age and sex of the patient, and that skin tension is directly related to the speed of the elastic wave [11]. We concluded that *in vivo* elastic wave measurements are a suitable method for inferring *in vivo* skin tension.

There exist analytical models relating the material properties to a surface wave speed. For example, for a Rayleigh surface wave travelling over a Mooney-Rivlin half space under uniform uniaxial tension, the wave speed is [21]:

$$v = \sqrt{\frac{E}{6\rho}\left[(1-\beta){\lambda_1}^2 + (1+\beta)\lambda_1\right]\left(1-(0.2956)^2{\lambda_1}^{-3}\right)}, \qquad (1)$$

where v is the wave speed along one axis, E is the Young's modulus, ρ is the density, β is a dimensionless material parameter which ranges from the neo-Hookean case ($\beta = -1$) to the extreme Mooney-Rivlin case ($\beta = +1$), see Section 2.2 for more details; λ_1 is the pre-stretch in the direction of tension.

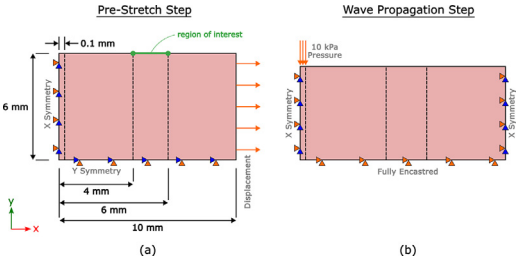

Fig. 1. Dimensions and boundary conditions of the FE model of wave propagation. (a) The uniaxial pre-stretch is generated using a displacement boundary condition, and (b) the wave is generated by a 10 kPa pressure applied for 2×10^{-5} s. The vertical displacement of the nodes in the 4 mm – 6 mm region was stored for analysis.

This analytical solution can be a useful tool, but, its real-world use is limited as it makes a number of assumptions and outputs a single wave which travels at a constant velocity. More recently, Li et al. developed an analytical solution that describes two propagating waves to account for the Rayleigh and supersonic shear waves [22]. Such analytical solutions can be useful for quantifying material parameters of interest using non-destructive means. Notably, Feng et al. developed a travelling-wave optical coherence elastography technique to measure the elastic modulus of the epidermis, dermis, and hypodermis [23]. However, to the best of our knowledge, there is no analytical method to determine the magnitude of skin tension, stress or pre-stretch.

It seems that, an objective method has not yet been developed that can non-invasively determine important subject specific parameters such as skin tension. As such, the overall objective of the paper is to present a method which can non-invasively identify the magnitude of *in vivo* skin tension and stress using surface wave speeds. To this goal, we have devised the following procedure, which constitutes the innovative contribution of this research:

1. Development of a simplified finite element (FE) model that simulates a typical surface wave propagation experiment in *in vivo* skin.
2. Creation of a large database of simulated test cases representative of real-world conditions.
3. Development of a statistical emulator for the purpose of a sensitivity analysis to elucidate the general trends and important features of surface wave propagation in *in vivo* skin.
4. Development of a machine learning (ML) model which can solve, in real time, the ill-posed and inverse problem of determining *in vivo* tension and stress from elastic wave speeds.

2. Materials and methods

2.1. Finite element modelling

The FE model for this study was designed to be both computationally inexpensive, as our analysis will involve running many simulations, and analogous to existing wave propagation devices (for example, the Reviscometer®).

We simulate a pre-stretched two-dimensional block of skin and impact the surface, see Fig. 1. This generates a wave that propagates along the surface of the skin. The vertical displacement of the nodes at known distances from the impact site can then be stored for analysis. To implement the model, firstly, the nonlinear FE package Abaqus/Standard (Dassault Systems, Waltham, MA) was used to statically pre-stretch the skin and, subsequently, Abaqus/Explicit (Dassault Systems, Waltham, MA) was used to perform the wave propagation. An assumption of plane stress was used for the FE simulations, in other words, there was no stress

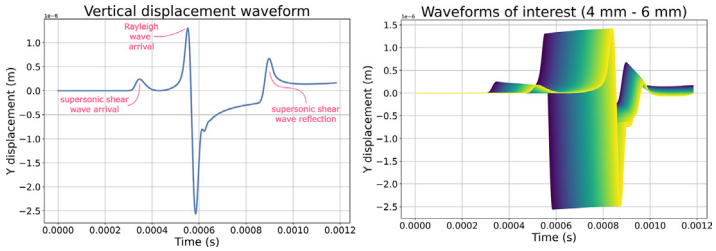

Fig. 2. Graph of the vertical displacement for (a) a node 4.8 mm away from the impact and (b) all nodes in the 4 mm - 6 mm region of interest. neo-Hookean material with a Young's modulus of 175 kPa, a density of 1,116 kg m^{-3} and a pre-stretch of 1.2 (20% extension).

"out-of-plane" in the z-direction. A four node plane stress element with reduced integration (CPS4R) was used to minimise computational complexity. The unstretched skin block has dimensions 10 mm × 6 mm and was discretised into 150,000 CPS4R elements with 150,801 nodes. The dimensions of the skin block were selected to minimise wave reflections interfering with waveforms from the region of interest (surface nodes 4 mm – 6 mm from the impact). The skin block is modelled by a hyperelastic material (either neo-Hookean or Mooney-Rivlin).

To perform the pre-stretch, a displacement boundary condition was used to perform a uniaxial stretch. After the pre-stretch, a wave was generated by applying a 10 kPa pressure for 2×10^{-5} s; see Fig. 1.

A typical y-displacement vs time graph 4.8 mm away from the applied perturbation is given in Fig. 2a. From these curves, important information about the speed of the elastic waves can be extracted and used to predict the material properties of the block of skin. For example, in Fig. 2 we see that a fast wave arrives just before 0.4 ms followed by a larger peak and corresponding trough occurring just before 0.6 ms. Finally, we can see a peak occurring around 0.9 ms, which is the result of the first wave reflecting off the bottom of the skin before reaching the node. The first wave is the supersonic shear wave, and the second (larger) wave is the Rayleigh surface wave (to be discussed further in Section 3.1).

The deformed coordinates of the nodes, i.e. their position after the pre-stretch step, can be used in conjunction with the arrival time of the wave to determine the wave velocity. However, this naive approach makes the implicit assumption that the wave is travelling at constant speed. It also requires precise knowledge about the wave generation method. For example, if a pressure is applied, it is necessary to know the precise area that the pressure was applied to as well as the duration of the perturbation.

By measuring multiple waveforms at different distances from the perturbation, see Fig. 2b, it is possible to extract more accurate measures of the wave speed while avoiding such assumptions. Finally, to avoid inherent discretisation errors when determining the arrival time of the "maximum" y-displacement, the waveform data points were interpolated by means of a quadratic spline function, as implemented in the Python function "InterpolatedUnivariateSpline" from the Python sub-package "scipy.interpolate" [24]. This smooth spline function passes through all data points and can be differentiated to find a more accurate arrival time of the waveform peak. Therefore, in our study, the speeds of the Rayleigh and supersonic shear waves (v_R and v_s) were taken to be the average of the wave speeds within the region of interest.

2.2. Input space sampling

Our goal was to train a ML model that could predict the material parameters of the skin using only the Rayleigh wave speed and supersonic shear wave speed described in Section 2.1. In order to have a model that is capable of accurate predictions for a wide variety of subjects with different combinations of material parameters, it was necessary to sample carefully from the input space.

We had to explore a four-dimensional input space of E, β, ρ and λ_1 (Young's modulus, beta, density and pre-stretch). To guarantee good coverage of this input space, a Latin hypercube sampling method [25] was employed. Specifically, the function "LatinHypercube" from the Python sub-package "scipy.stats.qmc" (Quasi-Monte Carlo) [24] was used to generate 5,000 samples using a neo-Hookean material model ($\beta = -1$) and an additional 5,000 samples using a Mooney-Rivlin material model. The material parameter ranges were chosen specifically to closely resemble those of *in vivo* human skin.

The neo-Hookean material model is hyperelastic and is commonly used to describe incompressible material response due to the simplicity of the form [26]. In Abaqus, its strain energy function U can be expressed as:

$$U = C_{10}\left(\bar{I}_1 - 3\right) + \frac{1}{D_1}\left(J_{el} - 1\right)^2, \tag{2}$$

where C_{10} and D_1 are material parameters, $\bar{I}_1$ is the reduced first strain invariant of the left Cauchy-Green tensor and J_{el} is the elastic volume strain [27]. C_{10} and D_1 can be related to the stiffness measured by the Young's modulus E and the incompressibility measured by the Poisson ratio ν by:

$$C_{10} = \frac{E}{6}, \qquad D_1 = \frac{9 - 18\nu}{E(1+\nu)}, \tag{3}$$

or, equivalently, to the shear modulus μ and bulk modulus k by [27]:

$$C_{10} = \frac{\mu}{2}, \qquad D_1 = \frac{2}{k}. \tag{4}$$

The Mooney-Rivlin material model can be viewed as an extension of the neo-Hookean form, as it adds a term that depends on the reduced second strain invariant $\bar{I}_2$ [27]. In Abaqus, its strain energy function can be expressed as:

$$U = C_{10}\left(\bar{I}_1 - 3\right) + C_{01}\left(\bar{I}_2 - 3\right) + \frac{1}{D_1}\left(J_{el} - 1\right)^2, \tag{5}$$

where C_{10}, C_{01} and D_1 are material parameters and J_{el} is the elastic volume strain. In this case, the initial Young's modulus E is expressed as [27]:

$$E = 6(C_{01} + C_{10}), \tag{6}$$

Therefore, to express the model parameters C_{10}, C_{01} and D_1 in terms of E and ν, a unitless parameter β is introduced:

$$C_{10} = \frac{E}{12}\left(1 - \beta\right), \qquad C_{01} = \frac{E}{12}\left(1 + \beta\right), \qquad \nu = \frac{9 - 18\nu}{E(1+\nu)}, \tag{7}$$

or, equivalently, the model parameters C_{10}, C_{01} and D_1 can be written in terms of μ and k:

$$C_{10} = \frac{\mu}{4}\left(1 - \beta\right), \qquad C_{01} = \frac{\mu}{4}\left(1 + \beta\right), \qquad D_1 = \frac{2}{k}, \tag{8}$$

where β ranges from -1, representing a pure neo-Hookean material, to $+1$, representing a pure Mooney-Rivlin case.

Table 1
Material property ranges used when sampling from the input space.

Material Property	Range	Units
E	[50, 300]	kPa
β	[−1, 1]	
ρ	[1060.2, 1171.8]	kg/m^3
λ_1	[1.05, 1.35]	

The density of skin ρ is often assumed to be a fixed value, for example the value 1116 kg/m^3 [28]. However, to allow for some variation due to hydration and other factors, we allowed the value to vary by ±5%. The skin's pre-stretch range in the principal direction λ_1 varies from study to study, depending on the measurement procedure. Jor et al. reported a maximum skin retraction of approximately 40% for porcine skin [19], Deroy et al. reported contractions in the 10% − 30% range for canine skin [10] and finally, Ní Annaidh et al. reported the mean failure strain of excised human skin to be 54% ± 17% [29]. For our study, a pre-stretch in the range from 5% to 35% was chosen.

The stiffness of human skin as measured by the Young's modulus E has been reported extensively using various methods. Liang and Boppart reported forearm skin to have $E \in [50, 150]$ kPa using optical coherence elastography [30], Li et al. reported values of the forearm dermis in the range $E \in [152.27, 286.68]$ kPa by measuring surface waves using optical coherence tomography [28], and Diridollou et al. reported forearm skin with $E \in [80, 260]$ kPa using a suction device [31]. As such, for our study, we selected a reasonably broad range of values between 50 kPa and 300 kPa. It should be noted here that while the Young's modulus is widely reported, there is a significant spread in the literature, due to variations in the location of the skin on the body, the method used to identify the Young's modulus and subject-specific attributes including age, sex, race, hydration, health etc. For instance, the review paper by Joodaki and Panzer [32] presents a summary of studies on the Young's modulus of whole skin, with measurements varying significantly. These variations range from 1.09 kPa (forearm of young female) as reported by Bader and Bowker [33] using an indentation test method, to tens of thousands of kPa reported by Grahame and Holt [34] using a suction device. Note that we used a fixed value for the Poisson ratio ($\nu = 0.495$) assuming all materials nearly incompressible [35–37].

In summary, 5,000 unique neo-Hookean and 5,000 unique Mooney-Rivlin subjects were generated with a Latin hypercube sampling technique using the material parameter ranges in Table 1. Two different material models were used to examine if the training and performance of the ML model were affected by the material model employed, i.e. the neo-Hookean and Mooney-Rivlin formulations, which are among the most common material models used for the breast [38]. For each subject, a FE simulation consisting of a static pre-stretch followed by a dynamic wave propagation technique (see Section 2.1) were performed, and the average Rayleigh and supersonic wave speeds were stored. This dataset was then used to train ML models of interest, as described in the subsequent sections.

2.3. Statistical emulation

A "simulator" is a mathematical representation of a physical system that is deterministic and computationally expensive, but is often the gold standard for replicating complex real-world behaviour [39–42]. For example, the gold standard method for determining the complex mechanical response of skin or other biological materials is a FE model. However, in practice, a three-dimensional FE simulation could take hours to run, making this method infeasible in many clinical settings, where an analysis needs to be performed quickly. Similarly, if it were of interest to see how small changes to each individual FE input affected the output (i.e. performing sensitivity analysis [43]), it would be necessary to run many FE simulations, which could be very computationally expensive.

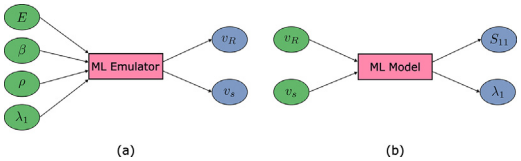

Fig. 3. Schematic of (a) the ML emulator used to relate the four input variables E, β, ρ and λ_1 (the Young's modulus, beta parameter, density and pre-stretch respectively), to the two output variables v_R and v_s (the Rayleigh wave speed and supersonic shear wave speed, respectively). (b) The ML model used to infer the steady-state stress, S_{11}, in the principal directions of stretch and the natural pre-stretch of the subject's skin, λ_1, from the input variables corresponding to the Rayleigh wave speed v_R and the supersonic shear wave speed v_s.

An "emulator" is a data-driven model that uses a training dataset of diverse outputs from the simulator to reconstruct the simulation outputs for unseen inputs in a relatively computationally inexpensive manner [39,41,42]. These cheap, fast, accurate approximations of the true simulator outputs can allow for clinical/real-world use, sensitivity analysis, efficient optimisation, uncertainty quantification, etc [39,41,42].

In our study, the simulator is the two-dimensional FE model described in Section 2.1, which has the material parameters of the skin as its inputs (E, ρ, λ_1 and β), and its outputs are the average Rayleigh and supersonic shear wave speeds (v_R and v_s) in the 4-6 mm region of interest; see Fig. 3. The training dataset for the emulator consists of the 10,000 input instances obtained from the Latin hypercube design for the various combinations of the input parameters (E, ρ, λ_1 and β), defined in Section 2.2, and the associated simulation velocity outputs (v_R and v_s). According to the value of β, the dataset is composed of 5,000 instances of neo-Hookean subjects and 5,000 Mooney-Rivlin subjects. While in principle many statistical and ML models can be employed as emulators (regression models, Gaussian process, random forests, support vector machines, neural networks etc.) [44–46], here we consider Gaussian process (GP) models [47] which allow for native uncertainty quantification and have been used by Stowers et al. in the context of predicting skin stress/strain for reconstructive surgeries [48]. Specifically, a Gaussian process regression model as implemented in "GaussianProcessRegressor" in the Python sub-package "sklearn.gaussian_process" was used [49]. The GP regression model was trained using a radial-basis function (RBF) kernel with length scale 1.0 as implemented in "RBF" in the Python sub-package "sklearn.gaussian_process.kernels" [49]. During the model training, the kernel hyperparameters were optimised using the "L-BFGS-B" algorithm from the Python sub-package "scipy.optimize.minimize" [24], following the implementation by Rasmussen and Williams [50]. To ensure the different magnitudes of the input variables (see Table 1) and output variables do not cause issues, all variables were rescaled to have mean 0 and standard deviation 1 prior to model training. An inverse transformation can easily be performed on the predictions from the trained GP model to obtain predictions in the natural units. Specifically, the function "StandardScaler" from the python sub-package "sklearn.preprocessing" was used to standardise the input and output variables [49]. The trained GP model was found to provide high predictive performance, and it also allows for uncertainty quantification by giving the mean and standard deviation as outputs when predicting, see Section 3.2. The Gaussian process pipeline and a sample of the ML training dataset can be found in the public GitHub repository accompa-

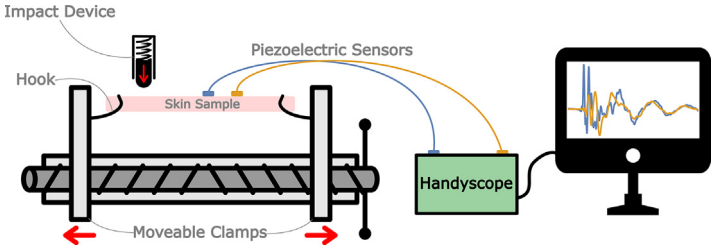

Fig. 4. Schematic of the experimental device used to collect wave speed measurements. The device consists of a synthetic tissue (Simulab) which is stretched uniaxially to a known pre-stretch value. A spring-loaded device provides the perturbation, and two piezoelectric sensors a known distance apart record the shape of the waveform for analysis.

nying this publication https://github.com/matt-nagle/A_Gaussian_process_approach_for_rapid_evaluation_of_skin_tension/.

2.4. Non-invasive prediction of material properties

As discussed in Section 1, there is a need to be able to measure the material properties of *in vivo* skin with a non-invasive procedure. In this study, we suggest that the speed of a surface wave travelling through the skin contains information about the material properties, which can be extracted. In theory, determining the wave speeds could be very straightforward, see Section 2.5. However, using these wave speeds to quantify stress and the pre-stretch *in vivo* requires solving a complex inverse problem in real time.

Similarly to the use of an emulator to reproduce the outputs of a computer simulation, we propose using a ML model as a computationally efficient way of solving the inverse problem of inferring stress and pre-stretch from the wave speeds. For this model, the velocity of the supersonic shear wave v_s and the Rayleigh wave speed v_R are now the input variables. The two target variables are the steady-state (after the pre-stretch but before the wave propagation) stress in the principal direction of stretch S_{11} and the natural pre-stretch of the subject's skin λ_1; see Fig. 3. These target variables were chosen as they are independent of the material model being used (unlike the Young's modulus E for example) and are the parameters of most interest in a surgical setting. The same dataset described in Section 2.3 obtained from the simulator is used for training, where in this case the inputs are (v_R, v_s) and the targets are (S_{11}, λ_1).

Again, while in principle this model could be of any form, in this case we consider a Gaussian process regression model with standardised inputs and outputs as it provided high predictive performance and also allowed for uncertainty quantification; see Section 3.3.

2.5. Experimental validation

To demonstrate that surface wave speed data of the type described in Section 2.1 can be collected easily and cheaply, a custom device was created consisting of two piezoelectric sensors and a custom uniaxial stretching apparatus, see Fig. 4.

The skin sample used was a synthetic tissue from Simulab (Seattle, USA), comprised of a single homogeneous layer of thickness 1 mm [51], designed to replicate human skin tissue. The uniaxial stretching apparatus consisted of a fixed base and two moving clamps mounted on a lead screw. The synthetic tissue was cut into strips with known dimensions 50 mm × 24 mm and secured to the clamps using a number of hooks that pierced through the skin. A known uniaxial pre-stretch could then be applied to the skin by rotating the lead screw.

A spring-loaded device was installed at a fixed distance above the skin sample, capable of providing repeatable perturbations normal to the surface of the skin, to generate a surface wave. To measure the shape of the waveform, two piezoelectric sensors (TE Connectivity Measurement Specialties) were fixed perpendicular to the direction of the uniaxial stretch, placed at a known distance apart and at a known distance from the impact site. The two sensors were connected to a Handyscope HS3-100 oscilloscope (TiePie Engineering), from which it was possible to visualise the voltage generated by the sensor as a function of time, see Fig. 5.

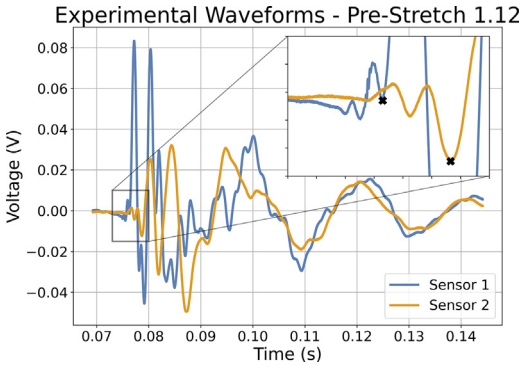

Fig. 5. Typical graph of Voltage vs Time from the two piezoelectric sensors. Synthetic tissue (Simulab) with a pre-stretch value of 1.12 (i.e. 12% stretch), the distance between the sensors was 17.13 mm. The most consistent results were found when comparing the voltage trough immediately before the main voltage peak, arrival times are marked in the inset plot with an "x".

Note that in Fig. 5 we see more oscillatory behaviour than in the FE model data (Fig. 2). This is likely due to wave reflection off the bottom of the skin sample and the inherently more complex surface wave propagation behaviour we would expect in three dimensions in a synthetic tissue sample. It should also be noted that it was only possible to extract information about the Rayleigh wave, as the supersonic wave was not visible. This may be due to wave attenuation or its smaller amplitude (see Fig. 2), making it more difficult to detect.

Using this setup, it was possible to experimentally determine the effect of pre-stretch on the surface wave velocity. Four pre-stretch values of 1.12, 1.19, 1.22 and 1.27 were considered, and five measurements were performed for each pre-stretch value. Note that the voltage-time waveforms obtained experimentally are analogous to the displacement-time graphs obtained from the FE simulations. Surface wave speed values were obtained by comparing the "arrival time" of particular features of the two waveforms and using the known distance between the piezoelectric sensors.

3. Results

3.1. Finite element results

As discussed in Section 2.1, the first step of each simulation was to perform a uniaxial static pre-stretch to simulate a pre-stressed

Fig. 6. Maximum principal stress (Pa) in the deformed neo-Hookean material with a Young's modulus of 175 kPa, a density of 1,116 kg m^{-3} and a pre-stretch of 1.2 (20% extension). This frame of the simulation was taken after 0.553 ms of wave propagation. The (larger) Rayleigh wave can be seen travelling along the surface of the skin, as well as the faster supersonic shear wave.

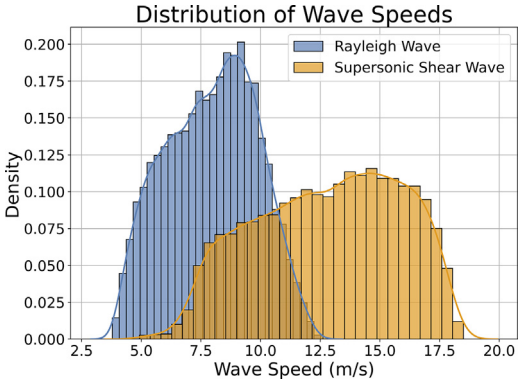

Fig. 7. Histograms of the distribution of the Rayleigh and supersonic shear wave speeds for all 10,000 subjects.

"*in vivo*" state before the wave was propagated along the surface of the skin. After the pre-stretch, a motion was generated through the skin, see Section 2.1. Both the Rayleigh and supersonic shear waves can be seen propagating through the material in Fig. 6.

After running all 10,000 simulations, it was found that the Rayleigh wave speed travelled between 3.78 and 12.53 m/s while the supersonic shear wave travelled between 4.9 and 18.5 m/s, with the supersonic shear wave always travelling faster than the Rayleigh wave. The distributions of the wave speeds are shown in Fig. 7. It should be noted here that the Rayleigh wave speeds from the FE simulation are in very good agreement with the predicted analytical results from Eq. (1) ($R^2 = 0.9951$). The analytical wave speeds are only slightly faster than the FE wave speeds, within 1.59% on average.

3.2. Statistical emulation results

The exact performance of any ML model is dependent on the train-test split of the data, i.e. which data points are used to train the model and which data points are withheld to test the performance of the trained model. So, to provide a fair assessment of the ability of the emulator to reproduce the simulator outputs, a 10-fold cross-validation procedure is implemented [52]. In the procedure, the dataset is randomly split into 10 folds of 1,000 subjects. In turn, each fold is used as a test set, while the other nine folds are employed to train the Gaussian process regression model. The mean of the R^2 [53] computed between estimated and simulation-outputted Rayleigh and supersonic velocities is employed as a metric to assess the predictive performance. This R^2 is averaged across the 10-fold replications, giving an average performance of 0.9993 ± 0.0003. This result indicates that the emulator is able to reproduce the simulation outputs in a stable manner to a very high degree of accuracy.

To get a visual indication of the predictive performance, we can consider one such 90%/10% train-test split, i.e. where one fold of the data is withheld as an unseen test set and the GP regression model is trained on the remaining nine folds. By comparing the simulation outputs to the predictions from the emulator for the unseen test set data points, we see that the emulator model is capable of reproducing very similar outputs to the simulator at a greatly reduced computational cost; see Fig. 8. Note that the GP model has slightly better predictive performance for the Rayleigh wave speed output as the Rayleigh wave has a larger amplitude (see Fig. 2) and is more stable than the supersonic shear wave speed, making it the "dominant" output.

Once trained, our emulator can be used to make predictions of Rayleigh and supersonic wave speeds for unknown sets of inputs in a fraction of the time it would take to run the full simulator. For example, a typical run of our FE simulation on a single CPU would take approximately 6 min (excluding data extraction and post-processing time). By contrast, a new prediction from the GP emulator takes approximately 30 milliseconds, a reduction in complexity of 4 orders of magnitude. With such a reduction in computing time, using the emulator, it is possible to perform a sensitivity analysis of the velocities as a function of ranges of the input parameters.

First, a large dataset was generated using the emulator, 20 equally spaced points were taken from the range of each input variable (E, ρ, β, λ_1), and each possible combination of points was considered, giving a dataset of 160 thousand observations. Following the method of sensitivity analysis from Section 7.2.2 of The Design and Analysis of Computer Experiments [42], two first order regression models were fitted:

$$v_R^* = \alpha_0^* + \alpha_1^* E^* + \alpha_2^* \rho^* + \alpha_3^* \beta^* + \alpha_4^* \lambda_1^*, \tag{9}$$

$$v_s^* = \alpha_0^* + \alpha_1^* E^* + \alpha_2^* \rho^* + \alpha_3^* \beta^* + \alpha_4^* \lambda_1^*, \tag{10}$$

where each variable x has been standardised as follows:

$$x^* = \frac{x - \bar{x}}{\sigma},$$

where $\bar{x}$ is the mean of x and σ is the standard deviation of x.

The regression coefficients α_i^* in Eqs. (9) and (10) are known as the standardised regression coefficients (SRCs). For example, α_1^* measures the change in our target variable (v_R^* or v_s^*) due to a unit standard deviation change in our input E. Because all variables are on a common scale after standardisation, the magnitude of the estimated SRCs tells us the relative sensitivity of the output to each input. The output is most sensitive to the input that has the largest absolute SRC value [42]. Table 2 shows the computed SRCs, where

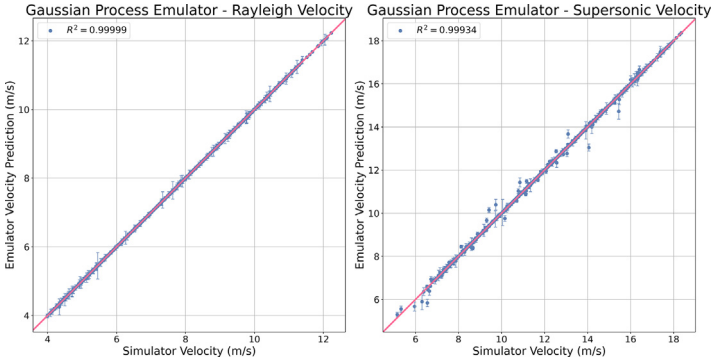

Fig. 8. Performance of the multi-output Gaussian process regression emulator, trained on 90% of the dataset and tested on the remaining unseen 10%. For each data point, the x coordinate is the "true" wave speed extracted from the FE simulation, the corresponding y coordinate is the GP prediction of the wave speed given the set of inputs E, β, ρ and λ_1 for that subject; the error bar is the 99% credible interval for the GP prediction. As shown, the emulator has extremely high predictive power.

Table 2
Standardised regression coefficients for Eqs. (9) and (10). Coefficients indicate that the velocity outputs are most sensitive to the Young's modulus E and are least sensitive to the density ρ. Note that this analysis is likely to be reasonable because the R^2 associated with the fitted models are 0.9796 and 0.9534 for v_R and v_s, respectively [42].

Input Variable	Estimated α_i^* (v_R)	Estimated α_i^* (v_s)
Young's Modulus (E)	0.9447	0.9328
Density (ρ)	−0.0609	−0.0621
Beta (β)	−0.1229	−0.2493
Pre-Stretch (λ_1)	0.2630	−0.1359

we see that the target variables are most sensitive to changes in the Young's modulus E and are least sensitive to changes in the density ρ. This result is consistent with Eq. (1) where we see that the Rayleigh wave speed is directly proportional to $\sqrt{E/\rho}$. Note that when sampling from the input space (see Section 2.2) we allowed E to have a much larger variation than ρ, which, in the literature, is often taken to be constant. Interestingly, we also see that the Rayleigh wave speed is more sensitive to λ_1 and less sensitive to β while conversely, the supersonic wave speed is more sensitive to β and less sensitive to λ_1.

A visual representation of the effect that each input variable has on the response wave speed can be obtained through conditional plots where all input are fixed at their mean and one variable is allowed to vary in its full range of values, see Fig. 9. The figures show that when the other material parameters are fixed at their mean and the Young's modulus is increased, both the Rayleigh and supersonic velocities also increase. Conversely, an increase in the density causes the wave speeds to decrease slightly (due to the relatively small amount of variance in density that was sampled). Interestingly, we see that there is a significant decrease in the supersonic wave speed in the transition from a pure neo-Hookean material ($\beta = -1$) to an extreme Mooney-Rivlin material ($\beta = +1$), whereas there is a much weaker decrease in the Rayleigh wave speed. We can also see that, as expected, the additional stretch causes the Rayleigh wave speed to increase significantly, but surprisingly, it causes the supersonic shear wave speed to decrease. This phenomenon has been demonstrated experimentally in a recent publication by Li et al., who performed uniaxial extension on a rubber sample at different magnitudes of pre-stress and observed the variations of the phase velocities of the Rayleigh and supershear waves [22].

While our emulator is performing the same task as Eq. (1), the ML method used is non-parametric, and as such, it is not possible to directly extract a simple equation which relates the material parameter inputs to the output velocities. However, it is possible to interpolate the complex relationship between our input variables (E, ρ, β and λ_1) and our output variables (v_R and v_s) that was learned by the Gaussian process emulator. The interpolation was performed using a parametric regression model. Specifically, the model "LinearRegression" from the Python sub-package "sklearn.linear_model" [49] was fit to the large dataset generated by the emulator during the sensitivity analysis, allowing us to extract the following equations:

$$v_R = -0.1519 - (3.8577 \times 10^{-11})E^2 + (3.7251 \times 10^{-5})E - (3.4424 \times 10^{-3})\rho - 0.3868\beta + 5.5120\lambda_1 \quad (11)$$

$$v_s = 15.8983 - (6.0573 \times 10^{-11})E^2 + (5.8806 \times 10^{-5})E - (5.6327 \times 10^{-3})\rho - 1.2569\beta - 4.5659\lambda_1 \quad (12)$$

Note that Eqs. (11) and (12) are simplifications of the true complex relationship between our variables. They are data-driven equations (not physics-derived, like Eq. (1)) that are conditional on the emulator model chosen and the FE model used to generate the simulator dataset. The R^2 values for the interpolation of Eqs. (11) and (12) are 0.9905 and 0.9637, respectively. This means that the simplified parametric equations are a good approximation of the non-parametric ML model.

3.3. Material property prediction results

As described in Section 2.4, a GP regression model was employed to predict steady state stress S_{11} in the principal direction of stretch and natural pre-stretch λ_1 of the subject's skin using the Rayleigh speed v_R and the supersonic speed v_s as inputs.

As in Section 3.2, we get a fair assessment of the ability of the GP regression model to predict the steady state stress S_{11} and the natural pre-stretch λ_1 by performing a 10-fold cross-validation procedure. The mean of the R^2 values computed for estimated and simulation-outputted steady-state stress S_{11} and natural pre-stretch λ_1 was employed as a metric to assess the predictive performance. This R^2 is averaged across the 10-fold replications, giving an average performance of 0.9570 ± 0.0025 when compared with the "true" values extracted from the FE simulations. From this, we can be confident that the predictive performance of the model is very strong and is not dependent on the initial split of the training and testing data.

Again, we get a visual indication of predictive performance by considering one such 90%/10% train-test split, i.e. where one fold of the data is withheld as an unseen test set and the GP regression model is trained on the remaining nine folds. By comparing the "true values" extracted from the FE simulations and the predictions from the GP model for the unseen test set data points, we see that the GP model is capable of accurate predictions of the stress and

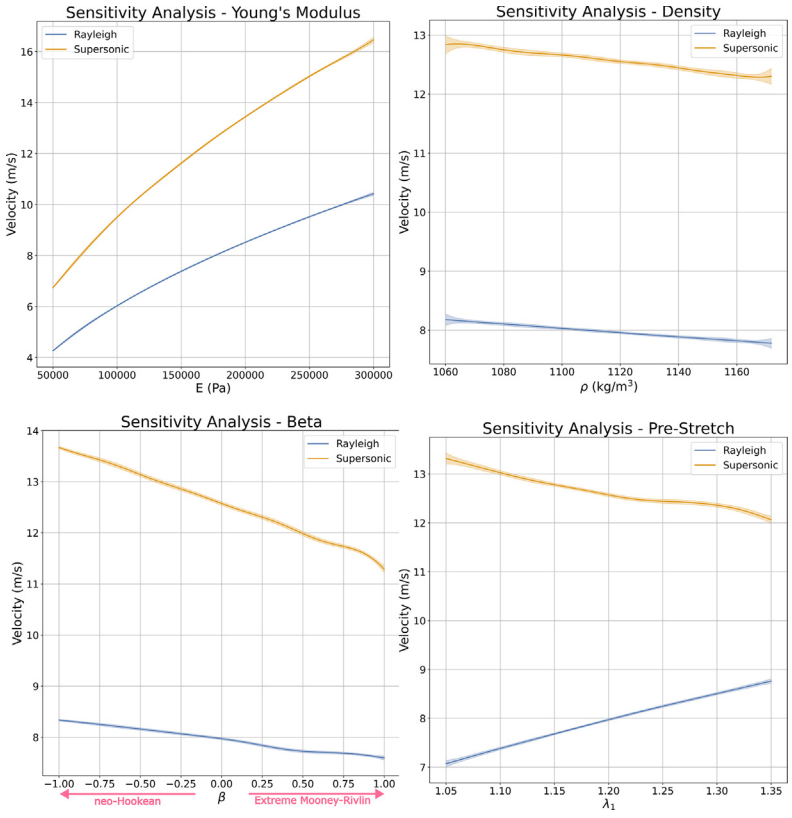

Fig. 9. Results of the sensitivity analysis where each input (a) E, (b) ρ, (c) β and (d) λ_1 was allowed to vary along their full range while each of the other input variables were held at their mean values, $E = 175$ kPa, $\beta = 0$, $\rho = 1,116$ kg m^{-3} and $\lambda_1 = 1.2$ (20% extension), and the effect on the output variables v_R and v_s was observed. The shaded region is the 99% credible interval for the GP prediction.

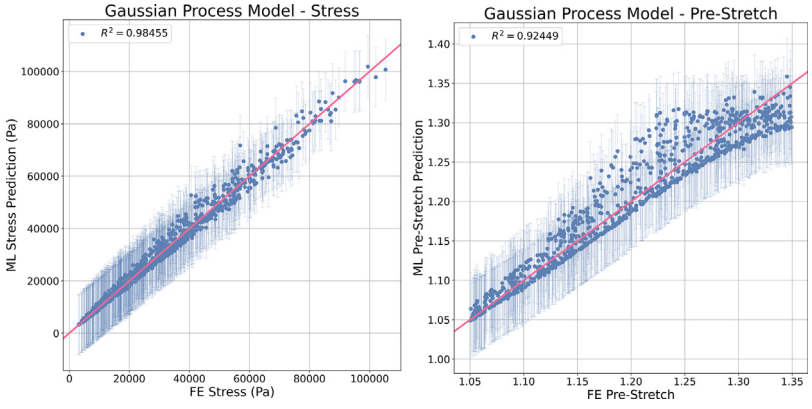

Fig. 10. Performance of the multi-output GP regression model trained on 90% of the dataset and tested on the remaining unseen 10%. For each data point, the x coordinate is the "true" stress/pre-stretch extracted from the FE simulation and the corresponding y coordinate is the GP prediction of the stress/pre-stretch given the wave speeds v_s and v_R. The error bar is the 99% credible interval for the GP prediction. As shown, the model has very strong predictive power for both output variables.

the pre-stretch of the skin using only the Rayleigh and supersonic wave speeds; see Fig. 10. Unsurprisingly, as the stress/stiffness in the material has the largest influence on the wave velocities (see Fig. 9), the model performs better at predicting the stress/stiffness, leading to a higher R^2 value. Interestingly, however, as the pre-stretch of the material has opposite effects on the Rayleigh and supersonic wave speeds (see Fig. 9d), the inclusion of the supersonic shear wave speed as an input to the GP model also allows accurate predictions of the pre-stretch. For comparison, the same GP model trained with the same train-test split with just a single input v_R is still capable of making reasonably accurate predictions of S_{11} ($R^2 = 0.8136$) but is incapable of accurate predictions of λ_1 ($R^2 = 0.1405$). We can also confirm this by performing the same sensitivity analysis procedure explained in Section 3.2 using the 10,000 measurements of v_R and v_s from the training dataset as our inputs. We see from the SRCs in Table 3 that while the Rayleigh wave speed is the most important, the supersonic wave speed has a noticeable level of importance in the GP model.

Table 3
Standardised regression coefficients for S_{11} and λ_1. Coefficients indicate that S_{11} and λ_1 are sensitive to both v_R and v_s.

Input Variable	Estimated α_i^* (S_{11})	Estimated α_i^* (λ_1)
Rayleigh wave speed (v_R)	1.8920	2.3758
Supersonic wave speed (v_s)	−1.1168	−2.2414

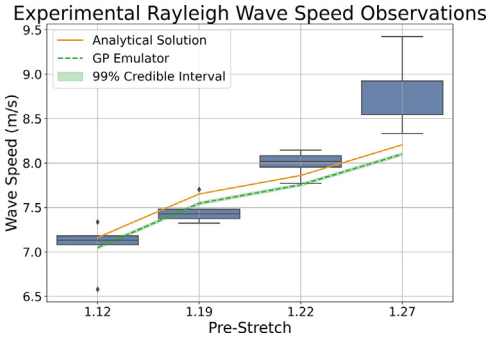

Fig. 11. Boxplots of the wave speeds measured experimentally for four different levels of pre-stretch. The GP emulator wave speed predictions and the analytical solution using Eq. (1) are in blue and orange respectively, where the synthetic tissue was assumed to be a neo-Hookean material ($\beta = -1$).

Again, we use our pre-trained GP model and our 10,000 combinations of ν_R and ν_s from the training data to extract a simplified parametric equation by fitting a regression model to interpolate the complex relationship between our input variables (ν_R and ν_s) and our output variables (S_{11} and λ_1):

$$S_{11} = 7639.4731 - 1163.2769\nu_R{}^2 - 3983.7169\nu_R - 1388.9624\nu_s{}^2 + 980.2333\nu_s + 3394.7445\nu_R\nu_s \quad (13)$$

$$\lambda_1 = 1.1925 - 0.0306\nu_R{}^2 + 0.1839\nu_R - 0.0084\nu_s{}^2 - 0.1150\nu_s + 0.0329\nu_R\nu_s \quad (14)$$

Again, note that Eqs. (13) and (14) are simplified data-driven approximations of the true complex relationship. As such, Eqs. (13) and (14) are conditional on the emulator model chosen and the FE model used to generate the simulator dataset. The R^2 values for the interpolation of Eqs. (13) and (14) are 0.9973 and 0.9540, respectively.

3.4. Experimental validation results

As discussed in Section 2.5, the experimental setup in Fig. 4 was used to take measurements of wave speed from a synthetic tissue sample for four levels of pre-stretch: 1.12, 1.19, 1.22 and 1.27. For each value of pre-stretch, five measurements were performed. The distribution of wave speeds for different levels of stretch can be seen in Fig. 11.

Overall, the wave speeds measured experimentally were consistent and repeatable, as demonstrated by the tight distributions for each value of pre-stretch in Fig. 11. The observed wave speeds were between 6.57 m/s and 9.43 m/s, consistent with the overall Rayleigh wave speed values obtained from the FE simulations, see Fig. 7. We also see that as the pre-stretch of the skin increases, the speed of the Rayleigh surface wave also increases. This behaviour is consistent with both the existing analytical solution and with our GP emulator, see Fig. 9 d. Furthermore, assuming that the neo-Hookean material ($\beta = -1$) model is suitable to describe the tissue sample, that the sample has uniform density ($\rho = 1116\,\mathrm{kg\,m^{-3}}$), and that the average Young's modulus measured by Kho et al. is correct ($E = 146\,\mathrm{kPa}$) [51], we can compare the experimentally measured wave speeds to the predictions from the pre-trained GP emulator described in Section 3.2 and the analytical solution from Eq. (1). We find that there is good agreement between the experimentally measured wave speeds and the predicted wave speeds up until the highest level of pre-stretch, where the GP emulator and the analytical solution deviate from the experimental results; see Fig. 11.

We can also visualise the relationship between the Rayleigh wave speed and the Young's modulus to examine the agreement between the FE dataset and the experimental observations, see Fig. 12a. There is a clear positive relationship between wave speed and Young's modulus: the higher the Young's modulus, the faster the Rayleigh wave speeds. For any fixed value of Young's modulus, a $1-3$ m/s variation in Rayleigh wave speed can be seen; this is due to different combinations of the other variables (pre-stretch, density and the material model). We see that the variation in wave speed observed in the experimental data is consistent with the variation expected from the FE data.

As discussed in Section 2.5, unfortunately, it was only possible to extract information about the Rayleigh wave speed, as the supersonic wave was not visible using the piezoelectric sensors employed. As such, it was not possible to validate the model presented in Section 2.4. Instead, we use the same FE dataset to train a new GP regression model which takes in as input the pre-stretch and the Rayleigh wave speed and predicts the Young's modulus of the skin ($R^2 = 0.9722$). It should be noted here that the real-world application of this model is limited, since in many cases the pre-stretch is unknown. Using this pre-trained model, we can input the pre-stretch and corresponding Rayleigh wave speed observations from the experimental data and obtain estimates for the Young's modulus of the synthetic skin sample, see Fig. 12b. The predictions from the GP regression model agree very well with the average Young's modulus of 146 kPa and fall within one standard deviation, measured by Kho et al. [51], which we would expect to vary due to hydration levels of the sample, variations in test set up, storage conditions etc. Thus, we have demonstrated a ML model trained solely on FE simulations is capable of accurate predictions of unknown material properties of interest using the pre-stretch and experimentally measured wave speeds from a simple wave propagation measurement.

4. Discussion

As demonstrated in Section 3.2, it is possible to train an emulator to quickly and accurately produce outputs similar to a more computationally expensive simulator, using some well-chosen input values. In practice, this advance can allow for exploration of the relationship between the input and output variables (for example in the form of a sensitivity analysis), or for real-world use where relying on the simulator would be too time-consuming. Note, it is reasonable to expect the skin material properties (i.e. the simulator inputs) to have a distribution centred around their population mean value in nature, for example the normal distribution. In this work, a Latin hypercube sampling method was employed to sample uniformly from the chosen range, resulting in an emulator which, in theory, is able to produce simulator outputs equally well over the entire input space.

When exploring the sensitivity of the emulator to the input variables, we found that the wave speeds are by far the most sensitive to the Young's modulus E and are not sensitive to the density ρ, see Table 2. This may initially seem at odds with Eq. (1), where we see the Rayleigh wave speed is directly proportional to $\sqrt{E/\rho}$. However, recall that when sampling from the input space (see Section 2.2) we allowed E to have a much larger variation than ρ (which in the literature is often taken to be constant), which is likely why for this emulator, the density ρ is not an important predictor.

In Section 3.3, we demonstrated that using a relatively simple GP model, it is possible to take wave speed data, which is easily accessible *in vivo*, and use it to accurately predict important material properties of the skin like the stress and the pre-stretch. While this model uses only two-dimensional FE data, it could be extended, incorporating three-dimensional FE and experimental data to allow for more accurate predictions of material properties *in vivo*. Given that the input parameters can be obtained easily and

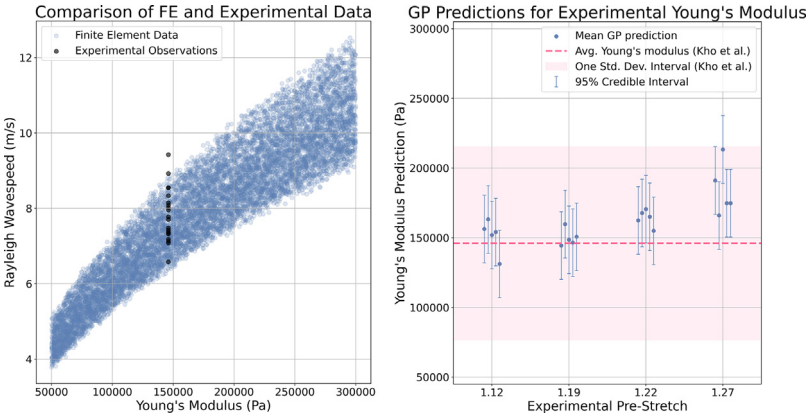

Fig. 12. (a) Scatter plot of the relationship between the Rayleigh wave speed and the Young's modulus for the FE data (blue) and the experimental observations (black). The experimental observations were all collected from synthetic tissue, with a Young's modulus of 146 kPa [51]. As shown, the experimental observations agree very well with the variation of wave speeds seen in the FE dataset. (b) Predictions from the pre-trained GP regression model using the experimental observations as inputs. Note that there is good agreement between the predicted Young's modulus from the GP model and the Young's modulus measured by Kho et al. [51].

non-invasively, this investigation offers a method which could be of real value to surgeons and patients.

For computational efficiency, a single homogeneous layer of skin was modelled in the FE simulations. While it is possible to model a more complex "multi-layer" skin block, in this work, this was not necessary as the goal of the FE simulation was to extract the speed of surface waves. As such, the material properties of the top layer of skin are the most important factor in the determination of the Rayleigh and supersonic wave speeds, the change in wave speed due to passing between skin layers will affect only the behaviour of the wave that is reflected off the bottom of the skin.

While our current dataset is based on simulated data, through this simulation approach, a number of implications for future physical measurements were identified:

1. We require at least one receiver, located a known distance away from the wave generating perturbation. However, more than one receiver is preferable and allows us to not be concerned with the specifics of the wave generation process.
2. We require enough sensitivity to be able to clearly identify the Rayleigh wave speed and ideally also the supersonic shear wave speed, which can give significant additional predictive power for S_{11} and λ_1.
3. Ideally, wave reflections should be identifiable and should not interfere with the supersonic and Rayleigh wave peak location.

In practice, this ML method could be viewed as an alternative to inverse FE procedures, which are a popular framework used in the literature to identify material properties [54–56]. Regular "forward" FE modelling involves inputting material properties, defining boundary conditions and loading conditions, etc., and receiving some output of interest. In the inverse FE framework, some output of interest is measured/obtained and the unknown value of interest is the material parameters. These quantities are often obtained through iterative rounds of FE simulations, where the material parameters are continuously tuned to minimise a predefined objective function to replicate the experimentally measured output [57]. The benefit of our approach is that all computational complexity is "front-loaded": once the input space has been explored, the FE simulations performed and the ML model trained, all subsequent predictions have extremely low computational cost. This makes our method much more suitable for real-time use where, for example, a trained and validated model could be deployed in a clinic where wave speed measurements can be taken and a near instantaneous prediction of material properties can be obtained with minimal expertise required. By contrast, with the inverse FE framework, any new observation requires new rounds of potentially computationally expensive FE simulations, and significant expertise to implement and interpret them.

There are a number of limitations to the method. First and foremost is that the trained model can only make predictions in the input space it has been trained on. As such, selection of the boundaries for the input space is of paramount importance when training a model that will be deployed in the real-world. Another limitation to the models presented here is that they have been trained entirely on simulated two-dimensional FE data. For this reason, there is no noise in the training dataset and the data generation process is entirely deterministic (i.e. multiple FE simulation runs with the same set of input variables will produce identical outputs). Thus, the models presented here may not generalise well to real-world observations where the data collection process is not perfect and the physical device used may have reduced resolution. The models presented here then should serve as a proof of concept and procedural outline by which models of this kind can be employed. In practice, once some experimental *in vivo* data has been collected, this simulated training dataset could be altered by reducing the precision and/or adding noise to make it more similar to the experimental observations. A more sophisticated model could then be developed by training on a combination of the adjusted FE data and experimental observations, which would likely generalise much better to the experimental data.

In this study, two different material models (neo-Hookean and Mooney-Rivlin), commonly used to model breast and other soft tissues, were used to examine if the ML model could still achieve high predictive performance while trained on a mix of material models. This proved to be a success: while models trained and tested on just the neo-Hookean or just the Mooney-Rivlin subjects had slightly higher performance, the model trained on the combined dataset still had very strong predictive power. The Mooney-Rivlin constitutive model was selected for this study, as it is the simplest model that depends on both the first and second strain invariants of the left Cauchy-Green tensor ($\bar{I}_1$ and $\bar{I}_2$). Thereby, it can often provide a good fit to experimental data whilst still retaining simplicity and requiring the fitting of fewer parameters. An additional benefit to the selection of neo-Hookean and Mooney-Rivlin material models is that they allowed for validation of the FE model using the existing analytical solution given in Equation 1. The FE model was developed as it allowed for the extraction of both the Rayleigh and supersonic shear wave speeds, providing a significant improvement in predictive performance. The full shape of the waveform could also be extracted and used directly for more

complex prediction tasks. Furthermore, the framework developed in this work is flexible and can easily be used for different material models where no analytical solution exists.

To demonstrate that wave speed measurements could be obtained cheaply and easily and be used to infer information about the pre-stretch, a custom experimental rig was designed consisting of a uniaxial tensioner, a spring-loaded device to impact the surface of the skin and two piezoelectric sensors to record the waveforms. As discussed in Section 3.4, the obtained Rayleigh wave speeds were consistent, repeatable, increased as expected with increasing pre-stretch, and had good agreement with existing analytical solutions and the GP emulator. By comparing the predicted Young's modulus from a newly-trained GP regression model to the Young's modulus measured by Kho et al. [51], see Fig. 12b, we demonstrate that a model trained solely on the FE simulations described in Section 2.1 is capable of fast and accurate predictions of skin material properties using wave speed observations from a simple and cheaply constructed wave propagation device.

However, it should be recognised here that there were a number of limitations to the experimental set-up. Firstly, the obtained waveforms only captured the Rayleigh surface wave and the supersonic shear wave was not visible. This may be due to the difference in amplitude between the Rayleigh and supersonic wave (see Fig. 2 a), sensitivity of the piezoelectric sensors and/or attenuation of the supersonic wave before arriving at the sensors, which was significantly further away from the impact location than in the FE simulation. It is also possible that the spring-loaded device used to generate the wave acted to increase attenuation of the perturbation. As such, it was not possible to validate the GP model presented in Section 3.3 and instead a new model was trained to demonstrate feasibility. This model used the pre-stretch and Rayleigh wave speed as inputs to predict the Young's modulus E. It should also be noted that while the Young's modulus prediction and general agreement between the experimental data and the GP emulator were very good for low/medium pre-stretch configurations, the wave speeds obtained from the higher stretch values, especially 1.27, were higher than expected. There are a number of experimental effects which may have led to this deviation, including delamination of the sensors from the skin surface or heterogeneous areas of strain at high stretches. It is also possible that the deviation is due to the non-linear stress-strain response of the synthetic tissue. Experimentally, the tissue was observed to experience wrinkling at high strain values (> 1.27) and as such it was not possible to obtain consistent wave speed measurements. Future work could involve a more thorough exploration of experimental wave speeds for different synthetic skin samples with different stiffnesses to quantify the effect that each material parameter has on the measured wave speed.

Finally, as discussed above, to generate the training data used in this study, a simplified two-dimensional FE simulation of fully elastic skin was used. Future work should involve extending this method into three dimensions. This would allow for the exploration of anisotropic skin tension through the use of a biaxial pre-stretch.

5. Conclusions

In this study, an innovative procedure was developed that provides real time non-invasive access to *in vivo* stretch and stress. First, a simplified FE model was developed to simulate surface wave propagation in *in vivo* skin. Then, a large dataset consisting of simulated real-world wave propagation experiments was constructed using the FE simulator. Using this dataset, a Gaussian process regression model was trained as an emulator that can replicate the FE model outputs with an average $R^2 = 0.9993$ at a 4 order of magnitude reduction in computational complexity. This allowed for sensitivity analysis of the physical parameters that affect the Rayleigh wave speed and supersonic shear wave speed. Then, a Gaussian process regression model was trained to solve the inverse problem of predicting clinically important material properties like the stress and the pre-stretch of *in vivo* skin using measurements of Rayleigh and supersonic wave speeds. This model was found to have an average $R^2 = 0.9570$ and furthermore it was possible to interpolate simplified parametric equations to calculate the stress and the pre-stretch. Finally, an experimental device consisting of two piezoelectric sensors and a spring-loaded impactor was used to take wave speed measurements at different degrees of pre-stretch from a sample of synthetic skin tissue (Simulab). These experimental wave speeds were shown to agree well with the existing analytical solution and the Gaussian process emulator. Furthermore, a ML model trained on just the FE data was capable of taking the experimental wave speeds as inputs and predicting a Young's modulus similar to that obtained from destructive mechanical characterisation tests. These results indicate that measuring surface wave speeds to predict skin pre-stretch and stress is a feasible method which could be employed in clinical settings to inform surgical procedures.

Declaration of competing interest

The authors declare that there is no conflict of interest. The authors declare that they have no known competing financial interests or personal relationships that could have appeared to influence the work reported in this paper.

CRediT authorship contribution statement

Matt Nagle: Conceptualization, Data curation, Formal analysis, Investigation, Methodology, Software, Visualization, Writing – original draft, Writing – review & editing. **Hannah Conroy Broderick:** Validation, Writing – review & editing, Methodology. **Christelle Vedel:** Data curation, Writing – review & editing. **Michel Destrade:** Validation, Writing – review & editing. **Michael Fop:** Conceptualization, Funding acquisition, Supervision, Writing – review & editing, Methodology. **Aisling Ní Annaidh:** Conceptualization, Funding acquisition, Supervision, Writing – review & editing, Methodology.

Acknowledgments

This publication has emanated from research supported in part by a Grant from Science Foundation Ireland under Grant number 18/CRT/6049. The opinions, findings and conclusions or recommendations expressed in this material are those of the authors and do not necessarily reflect the views of the Science Foundation Ireland. This work is partially supported by a Government of Ireland Postdoctoral Fellowship from the Irish Research Council (Project ID: GOIPD/2022/367). The authors wish to acknowledge the Irish Centre for High-End Computing (ICHEC) for the provision of computational facilities and support. Part of the graphical abstract was created with BioRender.com.

References

[1] E. Proksch, J.M. Brandner, J.-M. Jensen, The skin: an indispensable barrier, Exp. Dermatol. 17 (12) (2008) 1063–1072, doi:10.1111/j.1600-0625.2008.00786.x. Publisher: John Wiley & Sons, Ltd
[2] H.I.-C. Harn, R. Ogawa, C.-K. Hsu, M.W. Hughes, M.-J. Tang, C.-M. Chuong, The tension biology of wound healing, Exp. Dermatol. 28 (4) (2019) 464–471, doi:10.1111/exd.13460. Publisher: John Wiley & Sons, Ltd
[3] S. Paul, Biodynamic excisional skin tension lines for surgical excisions: untangling the science, Ann. R. Coll. Surgeons Engl. 100 (4) (2018) 330–337, doi:10.1308/rcsann.2018.0038.
[4] D. Son, A. Harijan, Overview of surgical scar prevention and management, J. Korean Med. Sci. 29 (6) (2014) 751–757, doi:10.3346/jkms.2014.29.6.751.

[5] N. Ziolkowski, S.C. Kitto, D. Jeong, J. Zuccaro, T. Adams-Webber, A. Miroshnychenko, J.S. Fish, Psychosocial and quality of life impact of scars in the surgical, traumatic and burn populations: a scoping review protocol, BMJ Open 9 (6) (2019) e021289, doi:10.1136/bmjopen-2017-021289.
[6] J.L. Azzi, C. Thabet, A.J. Azzi, M.S. Gilardino, Complications of tissue expansion in the head and neck, Head Neck 42 (4) (2020) 747–762, doi:10.1002/hed.26017. Publisher: John Wiley & Sons, Ltd
[7] G.C. Yalanis, S. Nag, J.R. Georgek, C.M. Cooney, M.A. Manahan, G.D. Rosson, J.M. Sacks, Mastectomy weight and tissue expander volume predict necrosis and increased costs associated with breast reconstruction, Plast. Reconstr. Surg. Global Open 3 (7) (2015), doi:10.1097/GOX.0000000000000408.
[8] K. Langer, On the anatomy and physiology of the skin: I. The cleavability of the cutis, Br. J. Plast. Surg. 31 (1) (1978) 3–8, doi:10.1016/0007-1226(78)90003-6.
[9] A.F. Borges, Relaxed skin tension lines (RSTL) versus other skin lines, Plast. Reconstr. Surg. 73 (1) (1984), doi:10.1097/00006534-198401000-00036.
[10] C. Deroy, M. Destrade, A. Aidan, A. Ni Annaidh, Non-invasive evaluation of skin tension lines with elastic waves, Skin Res. Technol. 23 (2017) 326–335, doi:10.1111/srt.12339.
[11] M. Nagle, S. Price, A. Trotta, M. Destrade, M. Fop, A. Ni Annaidh, Analysis of in vivo skin anisotropy using elastic wave measurements and Bayesian modelling, Ann. Biomed. Eng. 51 (8) (2023) 1781–1794, doi:10.1007/s10439-023-03185-2.
[12] A. Ni Annaidh, M. Destrade, Tension lines of the skin, in: G. Limbert (Ed.), Skin Biophysics: From Experimental Characterisation to Advanced Modelling, Springer International Publishing, Cham, 2019, pp. 265–280, doi:10.1007/978-3-030-13279-8_9.
[13] H. Seo, S.-j. Kim, F. Cordier, J. Choi, K. Hong, Estimating dynamic skin tension lines in vivo using 3D scans, Comput.-Aided Des. 45 (2) (2013) 551–555, doi:10.1016/j.cad.2012.10.044.
[14] D. Laiacona, J.M. Cohen, K. Coulon, Z.W. Lipsky, C. Maiorana, R. Boltyanskiy, E.R. Dufresne, G.K. German, Non-invasive in vivo quantification of human skin tension lines, Acta Biomater. 88 (2019) 141–148, doi:10.1016/j.actbio.2019.02.003.
[15] G. Boyer, L. Laquiéze, A. Le Bot, S. Laquiéze, H. Zahouani, Dynamic indentation on human skin in vivo: ageing effects, Skin Res. Technol. 15 (1) (2009) 55–67, doi:10.1111/j.1600-0846.2008.00324.x. Publisher: John Wiley & Sons, Ltd
[16] S.P. Paul, Biodynamic excisional skin tension lines for excisional surgery of the lower limb and the technique of using parallel relaxing incisions to further reduce wound tension, Plast. Reconstr. Surg. Global Open 5 (12) (2017), doi:10.1097/GOX.0000000000001614.
[17] E. Ruvolo Jr, G. Stamatas, N. Kollias, Skin viscoelasticity displays site- and age-dependent angular anisotropy, Skin Pharmacol. Physiol. 20 (6) (2007) 313–321, doi:10.1159/000108147.
[18] J. Dauendorffer, S. Bastuji-Garin, S. Guéro, N. Brousse, S. Fraitag, Shrinkage of skin excision specimens: formalin fixation is not the culprit, Br. J. Dermatol. 160 (4) (2009) 810–814, doi:10.1111/j.1365-2133.2008.08994.x.
[19] J.W.Y. Jor, M.P. Nash, P.M.F. Nielsen, P.J. Hunter, Estimating material parameters of a structurally based constitutive relation for skin mechanics, Biomech. Model. Mechanobiol. 10 (5) (2011) 767–778, doi:10.1007/s10237-010-0272-0.
[20] S.P. Paul, J. Matulich, N. Charlton, A new skin tensiometer device: computational analyses to understand biodynamic excisional skin tension lines, Sci. Rep. 6 (1) (2016), doi:10.1038/srep30117. Publisher: Springer Science and Business Media LLC
[21] J.N. Flavin, Surface waves in pre-stressed Mooney material, Q. J. Mech. Appl. Math. 16 (4) (1963) 441–449, doi:10.1093/qjmam/16.4.441.
[22] G.-Y. Li, X. Feng, A. Ramier, S.-H. Yun, Supershear surface waves reveal prestress and anisotropy of soft materials, J. Mech. Phys. Solids 169 (2022) 105085, doi:10.1016/j.jmps.2022.105085. Publisher: Elsevier BV
[23] X. Feng, G.-Y. Li, A. Ramier, A.M. Eltony, S.-H. Yun, In vivo stiffness measurement of epidermis, dermis, and hypodermis using broadband Rayleigh-wave optical coherence elastography, Acta Biomater. 146 (2022) 295–305, doi:10.1016/j.actbio.2022.04.030.
[24] P. Virtanen, R. Gommers, T.E. Oliphant, M. Haberland, T. Reddy, D. Cournapeau, E. Burovski, P. Peterson, W. Weckesser, J. Bright, S.J. van der Walt, M. Brett, J. Wilson, K.J. Millman, N. Mayorov, A.R.J. Nelson, E. Jones, R. Kern, E. Larson, C.J. Carey, I. Polat, Y. Feng, E.W. Moore, J. VanderPlas, D. Laxalde, J. Perktold, R. Cimrman, I. Henriksen, E.A. Quintero, C.R. Harris, A.M. Archibald, A.H. Ribeiro, F. Pedregosa, P. van Mulbregt, A. Vijaykumar, A.P. Bardelli, A. Rothberg, A. Hilboll, A. Kloeckner, A. Scopatz, A. Lee, A. Rokem, C.N. Woods, C. Fulton, C. Masson, C. Häggström, C. Fitzgerald, D.A. Nicholson, D.R. Hagen, D.V. Pasechnik, E. Olivetti, E. Martin, E. Wieser, F. Silva, F. Lenders, F. Wilhelm, G. Young, G.A. Price, G.-L. Ingold, G.E. Allen, G.R. Lee, H. Audren, I. Probst, J.P. Dietrich, J. Silterra, J.T. Webber, J. Slavič, J. Nothman, J. Buchner, J. Kulick, J.L. Schönberger, J.V. de Miranda Cardoso, J. Reimer, J. Harrington, J.L.C. Rodriguez, J. Nunez-Iglesias, J. Kuczynski, K. Tritz, M. Thoma, M. Newville, M. Kümmerer, M. Bolingbroke, M. Tartre, M. Pak, N.J. Smith, N. Nowaczyk, N. Shebanov, O. Pavlyk, P.A. Brodtkorb, P. Lee, R.T. McGibbon, R. Feldbauer, S. Lewis, S. Tygier, S. Sievert, S. Vigna, S. Peterson, S. More, T. Pudlik, T. Oshima, T.J. Pingel, T.P. Robitaille, T. Spura, T.R. Jones, T. Cera, T. Leslie, T. Zito, T. Krauss, U. Upadhyay, Y.O. Halchenko, Y. Vázquez-Baeza, SciPy 1.0 Contributors, SciPy 1.0: fundamental algorithms for scientific computing in Python, Nat. Methods 17 (3) (2020) 261–272, doi:10.1038/s41592-019-0686-2.
[25] M.D. McKay, R.J. Beckman, W.J. Conover, A comparison of three methods for selecting values of input variables in the analysis of output from a computer code, Technometrics 21 (2) (1979) 239–245, doi:10.2307/1268522.
[26] D. Behera, P. Roy, E. Madenci, Peridynamic correspondence model for finite elastic deformation and rupture in Neo-Hookean materials, Int. J. Non-Linear Mech. 126 (2020) 103564, doi:10.1016/j.ijnonlinmec.2020.103564.
[27] M. Smith, ABAQUS/Standard User's Manual, Version 6.9, Dassault Systémes Simulia Corp, United States, 2009.
[28] C. Li, G. Guan, R. Reif, Z. Huang, R.K. Wang, Determining elastic properties of skin by measuring surface waves from an impulse mechanical stimulus using phase-sensitive optical coherence tomography, J. R. Soc. Interface 9 (70) (2011) 831–841, doi:10.1098/rsif.2011.0583. Publisher: Royal Society
[29] A. Ni Annaidh, K. Bruyére, M. Destrade, M.D. Gilchrist, M. Otténio, Characterization of the anisotropic mechanical properties of excised human skin, J. Mech. Behav. Biomed. Mater. 5 (1) (2012) 139–148, doi:10.1016/j.jmbbm.2011.08.016.
[30] X. Liang, S. A. Boppart, Biomechanical properties of in vivo human skin from dynamic optical coherence elastography, IEEE Trans. Biomed. Eng. 57 (4) (2010) 953–959, doi:10.1109/TBME.2009.2033464.
[31] S. Diridollou, V. Vabre, M. Berson, L. Vaillant, D. Black, J.M. Lagarde, J.M. Grégoire, Y. Gall, F. Patat, Skin ageing: changes of physical properties of human skin in vivo, Int. J. Cosmet. Sci. 23 (6) (2001) 353–362, doi:10.1046/j.0412-5463.2001.00105.x. Publisher: John Wiley & Sons, Ltd
[32] H. Joodaki, M.B. Panzer, Skin mechanical properties and modeling: A review, Proc. Inst. Mech. Eng. Part H J. Eng. Med. 232 (4) (2018) 323–343, doi:10.1177/0954411918759801.
[33] D.L. Bader, P. Bowker, Mechanical characteristics of skin and underlying tissues in vivo, Biomaterials 4 (4) (1983) 305–308, doi:10.1016/0142-9612(83)90033-9.
[34] R. Grahame, P. Holt, The influence of ageing on the in vivo elasticity of human skin, Gerontologia 15 (2-3) (2009) 121–139, doi:10.1159/000211681.
[35] R. Sanders, Torsional elasticity of human skin in vivo, Pflügers Archiv. 342 (3) (1973) 255–260, doi:10.1007/BF00591373.
[36] F.M. Hendriks, D. Brokken, J.T.W.M. Van Eemeren, C.W.J. Oomens, F.P.T. Baaijens, J.B.A.M. Horsten, A numerical-experimental method to characterize the non-linear mechanical behaviour of human skin, Skin Res. Technol. 9 (3) (2003) 274–283, doi:10.1034/j.1600-0846.2003.00019.x. Publisher: John Wiley & Sons, Ltd
[37] R. Reihsner, B. Balogh, E.J. Menzel, Two-dimensional elastic properties of human skin in terms of an incremental model at the in vivo configuration, Med. Eng. Phys. 17 (4) (1995) 304–313, doi:10.1016/1350-4533(95)90856-7.
[38] A.M. Teixeira, P. Martins, A review of bioengineering techniques applied to breast tissue: mechanical properties, tissue engineering and finite element analysis, Front. Bioeng. Biotechnol. 11 (2023) 1161815, doi:10.3389/fbioe.2023.1161815.
[39] L.S. Bastos, A. O'Hagan, Diagnostics for Gaussian Process Emulators, Technometrics 51 (4) (2009) 425–438, doi:10.1198/TECH.2009.08019. Publisher: Taylor & Francis _eprint:
[40] J. Sacks, W.J. Welch, T.J. Mitchell, H.P. Wynn, Design and analysis of computer experiments, Stat. Sci. 4 (4) (1989) 409–423, doi:10.1214/ss/1177012413. Publisher: Institute of Mathematical Statistics
[41] R.B. Gramacy, Surrogates: Gaussian Process Modeling, Design, and Optimization for the Applied Sciences, Chapman and Hall/CRC, 2020, doi:10.1201/9780367815493.
[42] T.J. Santner, B.J. Williams, W.I. Notz, The design and analysis of computer experiments, Springer series in statistics, Springer, New York, NY, 2010, doi:10.1007/978-1-4757-3799-8.
[43] S. Razavi, A. Jakeman, A. Saltelli, C. Prieur, B. Iooss, E. Borgonovo, E. Plischke, S.L. Piano, T. Iwanaga, W. Becker, S. Tarantola, J.H.A. Guillaume, J. Jakeman, H. Gupta, N. Melillo, G. Rabitti, V. Chabridon, Q. Duan, X. Sun, S. Smith, R. Sheikholeslami, N. Hosseini, M. Asadzadeh, A. Puy, S. Kucherenko, H.R. Maier, The future of sensitivity analysis: an essential discipline for systems modeling and policy support, Environ. Modell. Softw. 137 (2021) 104954, doi:10.1016/j.envsoft.2020.104954.
[44] N. Villa-Vialaneix, M. Follador, M. Ratto, A. Leip, A comparison of eight metamodeling techniques for the simulation of N2O fluxes and N leaching from corn crops, Environ. Modell. Softw. 34 (2012) 51–66, doi:10.1016/j.envsoft.2011.05.003.
[45] R. Zhang, C. Wu, A.T.C. Goh, T. Böhlke, W. Zhang, Estimation of diaphragm wall deflections for deep braced excavation in anisotropic clays using ensemble learning, Geosci. Front. 12 (1) (2021) 365–373, doi:10.1016/j.gsf.2020.03.003.
[46] A. Bhosekar, M. Ierapetritou, Advances in surrogate based modeling, feasibility analysis, and optimization: a review, Comput. Chem. Eng. 108 (2018) 250–267, doi:10.1016/j.compchemeng.2017.09.017.
[47] C.E. Rasmussen, Gaussian processes in machine learning, in: O. Bousquet, U. von LuLuxburgxburg, G. Rätsch (Eds.), Advanced Lectures on Machine Learning: ML Summer Schools 2003, Canberra, Australia, February 2 - 14, 2003, Tübingen, Germany, August 4 - 16, 2003, Revised Lectures, Springer Berlin Heidelberg, Berlin, Heidelberg, 2004, pp. 63–71, doi:10.1007/978-3-540-28650-9_4.
[48] C. Stowers, T. Lee, I. Bilionis, A.K. Gosain, A.B. Tepole, Improving reconstructive surgery design using Gaussian process surrogates to capture material behavior uncertainty, J. Mech. Behav. Biomed. Mater. 118 (104340) (2021) 104340. Publisher: Elsevier BV
[49] F. Pedregosa, G. Varoquaux, A. Gramfort, V. Michel, B. Thirion, O. Grisel, M. Blondel, P. Prettenhofer, R. Weiss, V. Dubourg, J. Vanderplas, A. Passos, D. Cournapeau, M. Brucher, M. Perrot, E. Duchesnay, Scikit-learn: machine learning in Python, J. Mach. Learn. Res. 12 (85) (2011) 2825–2830.
[50] C.E. Rasmussen, C.K.I. Williams, Gaussian Processes for Machine Learning, The MIT Press, 2005, doi:10.7551/mitpress/3206.001.0001.

[51] A.S.K. Kho, S. Béguin, E.D. O'Cearbhaill, A.N. Annaidh, Mechanical characterisation of commercial artificial skin models, J. Mech. Behav. Biomed. Mater. 147 (2023) 106090, doi:10.1016/j.jmbbm.2023.106090.
[52] T. Hastie, R. Tibshirani, J. Friedman, The Elements of Statistical Learning, Springer New York, 2009, doi:10.1007/978-0-387-84858-7.
[53] C. Lewis-Beck, M. Lewis-Beck, Applied Regression: An Introduction, Quantitative Applications in the Social Sciences, SAGE Publications, 2015.
[54] H.A. Nieuwstadt, S. Fekkes, H.H.G. Hansen, C.L.d. Korte, A.v.d. Lugt, J.J. Wentzel, A.F.W.v.d. Steen, F.J.H. Gijsen, Carotid plaque elasticity estimation using ultrasound elastography, MRI, and inverse FEA - A numerical feasibility study, Med. Eng. Phys. 37 (8) (2015) 801–807, doi:10.1016/j.medengphy.2015.06.003.
[55] R.A. Baldewsing, M.G. Danilouchkine, F. Mastik, J.A. Schaar, P.W. Serruys, A.F.W. van der Steen, An inverse method for imaging the local elasticity of atherosclerotic coronary plaques, IEEE Trans. Inf. Technol. Biomed. 12 (3) (2008) 277–289, doi:10.1109/TITB.2007.907980.
[56] A.D. Pant, L. Kagemann, J.S. Schuman, I.A. Sigal, R. Amini, An imaged-based inverse finite element method to determine in-vivo mechanical properties of the human trabecular meshwork, J. Model. Ophthalmol. 1 (3) (2017) 100–111.
[57] B. Narayanan, M.L. Olender, D. Marlevi, E.R. Edelman, F.R. Nezami, An inverse method for mechanical characterization of heterogeneous diseased arteries using intravascular imaging, Sci. Rep. 11 (1) (2021) 22540, doi:10.1038/s41598-021-01874-3.